Article

Design and Manufacture of Composite Landing Gear for a Light Unmanned Aerial Vehicle

Yen-Chu Liang [1,*], Pei-Chieh Chin [2], Yun-Ping Sun [3] and Muh-Rong Wang [2]

1. Department of Aeronautics and Astronautics, Chinese Air Force Academy, Kaohsiung 820111, Taiwan
2. Department of Aeronautics and Astronautics, National Cheng Kung University, Tainan 701401, Taiwan; pcchin@mail.ncku.edu.tw (P.-C.C.); wangmr@mail.ncku.edu.tw (M.-R.W.)
3. Department of Mechanical Engineering, Cheng Shiu University, Kaohsiung 83301, Taiwan; ypsun@gcloud.csu.edu.tw
*   Correspondence: agcafa221@yahoo.com.tw

Abstract: Unmanned aerial vehicles (UAVs) have become popular for military applications as well as for use in structural inspection, weather monitoring, and festival demonstrations. Suitable landing gears to ensure that the UAV can take off and land safely are important when the price of the cargo and UAV increase. A lightweight and high-strength landing gear is desirable to overcome accidents during service. Composite materials are a promising, excellent solution for this purpose. This study demonstrated the design, numerical analysis (Ansys), manufacture, and experimental verification (LabVIEW) of a composite landing gear for a UAV. In particular, landing gears with different carbon fiber-reinforced polymer (CFRP) composite fiber orientations were analyzed, manufactured, and experimentally verified in this study.

1. Introduction

Unmanned aerial vehicles (UAVs) have been used worldwide for industrial applications such as surveying objects and the ground using orthographic photos, volume calculations, digital height, and 3D models. Recent advances and challenges in road safety, traffic, and highway infrastructure management by using UAVs or through cooperation with ground unmanned vehicles can be found in [1,2]. The integration of UAVs in smart cities is very challenging owing to issues and concerns related to safety, privacy, and ethical/legal use [3]. The false alarms of forest fires may be reduced by using the detection and monitoring system of UAVs [4]. In military applications, an unmanned combat aerial vehicle (UCAV) can carry aircraft ordnance such as missiles to perform drone strikes. For example, the X-47B has a wingspan of 18.9 m, a cruise range of 3889 km, and a maximum gross take-off weight of 20 t, and it can carry a payload of 2 t. The charging of UAVs may be solved by solar energy or wireless power. Another critical goal is to reduce the weight of UAVs. An efficient method to do so is to develop and use composite materials.

Composite materials contain both fibers and resin and therefore show excellent characteristics including low density, high strength, anti-corrosion and anti-fatigue properties, and ease of construction and repair. Composite materials therefore find wide applications in aeronautical industries, medical fields, sports equipment, cars and boats, and construction industries. In particular, they are used in aerial vehicles to reduce the weight and thereby reduce fuel consumption. Furthermore, they show high endurance in space applications. Composite materials have a Young's modulus two times that of conventional metals and aluminum alloys with half the weight [5]. Newly developed composite materials are attracting commercial interest for applications in next-generation aircrafts.

Composite structures are widely used in small UAV structures. Studies have reported on the challenges and advantages of composite materials when used for the design and fabrication of UAVs [6,7]. In 2003, SP-Aerospace produced the first metal-based composite landing gear and evaluated it in terms of cost savings and weight reduction. The National Aerospace Laboratory (NLR) [8] evaluated the components of a composite landing gear and reported 20% weight reduction, 15% lower manufacturing costs, and reduced lead time. Park et al. conducted a finite element analysis using NASTRAN for the wing and landing gear of a composite drone air vehicle [9]. They applied forces of 5 g and −1.5 g to the wing and 2 g to the main landing gear. They found that a 40-layer design of $[45/0/-45/90]_{5S}$ with 7.6-mm thickness is the optimal solution for the structure. To identify the possibility of other landing cases, vertical landing forces of 36, 120, and 240 N were performed and obtained the maximum stresses of 48, 129, and 911 MPa, respectively. The safety factor was 2, though the non-smooth shape of the landing gear results in stress concentration. Kshittij presented a composite skid landing gear design for a helicopter in 2009 [10]. $[0/75/-75]_{8S}$ and $[0/45/-45]_{8S}$ designs for composite landing gears with 48 multilayers of mixed alloys were proposed. Fractures occurred at the alloy–composite interface when the helicopter was in service. The $[0/45/-45]_{8S}$ design showed less damage. Pitatzis et al. presented strategic design steps for the structural optimization of a UAV. An interactive parameterized method led to significant (>30%) airframe weight reduction between the initial coarse and the final optimized structural configurations [11]. The landing gear was not made of composite materials. Instead, A17075-T6 aluminum alloy was used with certain structural design changes to reduce the weight of the landing gear. The final optimal main landing gear shape had corners that may increase the stress concentration. Thompson et al. designed and constructed a 5-m wingspan, fully composite blended wing body UAV [12]. It had a gross weight of 25 kg and could carry a payload of 50 kg. The aerodynamics and static structures were simulated using Ansys for landing with a force of 10 g, and the landing gear structure failed for the design, having a 45° orientation of fibers in the layers. Airoldi et al. presented shape variation capabilities in camber wing structures with flexible morphing parts [13]. Landing gear made of glass fiber, carbon fiber, and epoxy resin for an aerial target with a gross weight of 30 kg was simulated and manufactured by Ciobanu et al. [14]. The materials used were not prepregs and the thickness was variable from 5 mm at the ends to 9 mm in the central zone. The analysis of the behavior of the main landing gear for a payload of 3 g impact loading (900 N) was simulated and obtained a maximum stress of 149 MPa. The mass of the landing gear was in the range of 775 to 876 g. This is too heavy for a light UAV. The strength and weight of the UAV are the main considerations for the additional weight required from the functional payload. Therefore, future development in composites will have many different types for different UAVs.

The design of the landing gear focuses on weight reduction and strength enhancement through the selection of proper prepregs' plies and orientation design. In this study, a composite landing gear for a light UAV is designed, analyzed, and manufactured. A curved landing gear was designed for a small UAV with 5-kg weight and 10-kg maximum payload. The payload:weight ratio was, therefore, 2. The design parameters of the carbon fiber-reinforced polymer (CFRP) landing gear were the number of layers and the fiber orientations. The CFRP landing gear was manufactured, and experiments including signal acquisition using LabVIEW and loading system operation using a material test stand (MTS) were conducted. The results show that the experimentally measured and the simulated strains are in good agreement and that the designed landing gear is safe under the constraint of a safety factor of 3.

2. Design of Landing Gear

The forces applied on an aircraft are weight, lift, thrust, and drag. The position of the center of gravity may change slightly as fuel is utilized. The magnitude and direction of the lift, thrust, and drag forces always change when the velocity and attitude of the aircraft change. Figure 1 shows the three loading scenarios for the landing gear when an

aircraft takes off or lands; the ideal scenario is shown in Figure 1a. All loads are distributed smoothly on the nose gear and the main landing gears (the orange dot lines). However, not all forces applied on the aircraft keep the attitude ideal. For example, accidents may occur in the scenarios shown in Figure 1b, c when side forces applied by wind disturb the attitude of the aircraft. UAVs use one of three landing gear designs: tail wheel type, tandem type, and tricycle type [15]. The tricycle-type design is used very frequently because it makes the UAV easily maneuverable. Its other advantages include optimal location of center of gravity, evenly distributed weight of UAV, small effect of crosswind, and easy maneuverability. Its disadvantages include increased drag, slightly higher weight, and tendency to damage the nose gear [15]. Nonetheless, the tricycle-type landing gear was chosen in this study.
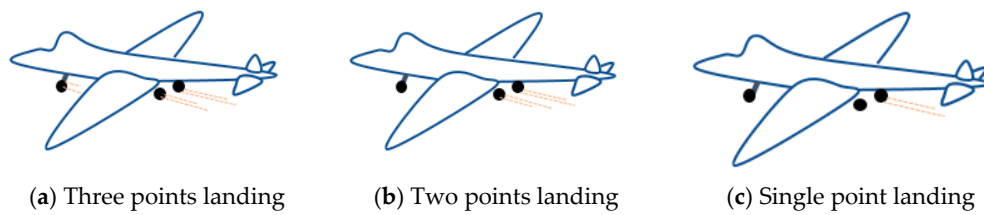

(**a**) Three points landing   (**b**) Two points landing   (**c**) Single point landing

Figure 1. Situations of aircrafts' take-off or landing.

This paper presents the design, simulation, manufacturing, and testing of UAV landing gear with a view to increasing its strength and operational life and decreasing its cost. The safety factor is 3, the aircraft weight is 5 kg, and the payload is 10 kg. First, the landing gear should not have sharp corners to avoid stress concentration and failure during service, as shown in Figure 2. The landing gear is made of CFRP and has 12 zero-degree layers. The maximum principal stress is 136.28 MPa with the corner design, as shown in Figure 2a. The maximum principal stress is 69.7 MPa with the curved design, shown in Figure 2b. Therefore, the stress concentration with the corner design is nearly two times that with the curved design. The span of the landing gear cannot be too large to fit the fuselage and runway. However, it should be large enough to overcome variations in the center of gravity. The wingspan is approximately 3 m. The landing gear has dimensions of $30 \times 9 \times 5.5$ cm^3, as shown in the three-view plot in Figure 3. Table 1 shows the (x, y, z) coordinates of the designed shape in Figure 3. The first column indicates the group number (GN); the second column, the node number (NN); and the third, fourth, and fifth columns, the x, y, and z coordinates of the landing gear, respectively. This format is used for the coordinate file imported into Ansys. Figure 4 shows the landing gear geometry as simulated in Ansys; the (x, y, z) coordinates are defined in the bottom right corner.
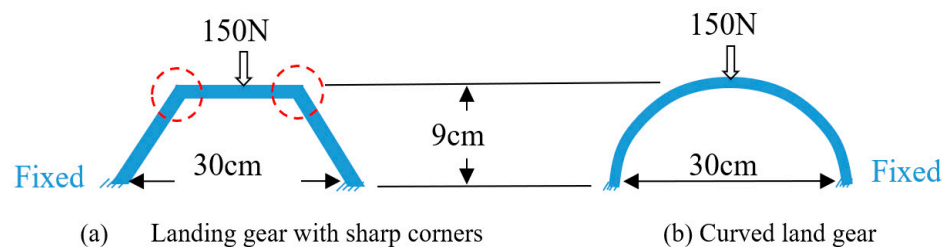

(a)   Landing gear with sharp corners   (b) Curved land gear

Figure 2. Shapes of unmanned aerial vehicle's (UAV) landing gear.
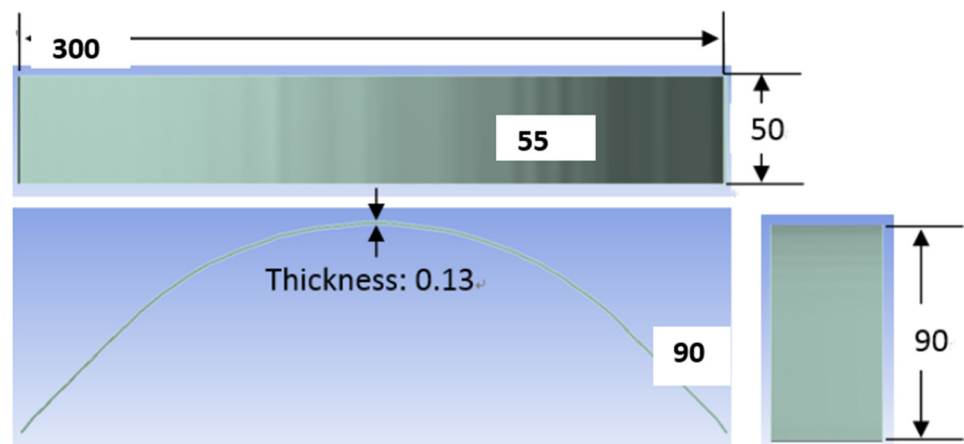
Figure 3. Three-view plot of UAV landing gear (unit: mm).

Table 1. Information of landing gear in 2D.

| GN	NN	x	y	z	GN	NN	x	y	z
1	1	−150	0	0	1	17	10	89.61	0
1	2	−140	12.63	0	1	18	20	88.42	0
1	3	−130	23.29	0	1	19	30	86.45	0
1	4	−120	33.16	0	1	20	40	83.68	0
1	5	−110	42.24	0	1	21	50	80.13	0
1	6	−100	50.53	0	1	22	60	75.79	0
1	7	−90	58.03	0	1	23	70	70.66	0
1	8	−80	64.74	0	1	24	80	64.74	0
1	9	−70	70.66	0	1	25	90	58.03	0
1	10	−60	75.79	0	1	26	100	50.53	0
1	11	−50	80.13	0	1	27	110	42.24	0
1	12	−40	83.68	0	1	28	120	33.16	0
1	13	−30	86.45	0	1	29	130	23.29	0
1	14	−20	88.42	0	1	30	140	12.63	0
1	15	−10	89.61	0	1	31	150	0	0
1	16	0	90	0					
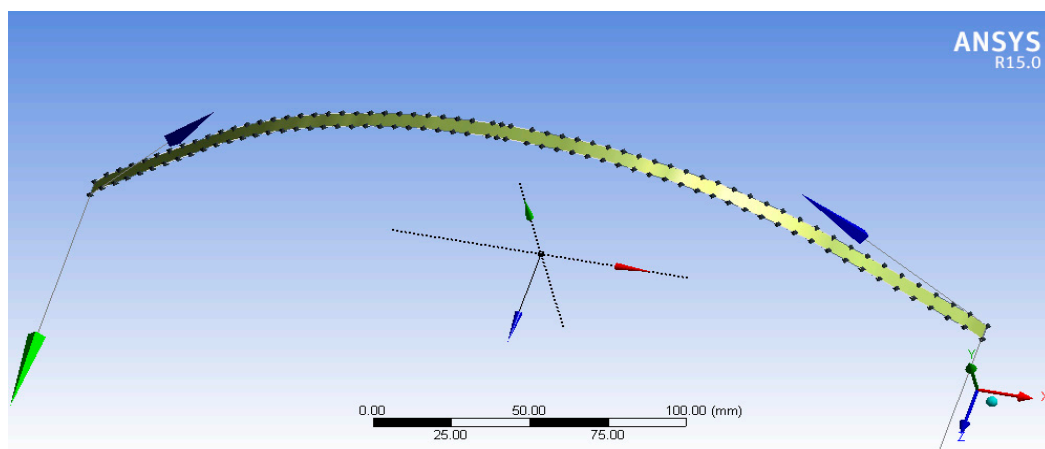
Figure 4. Geometry of UAV landing gear.

3. Static Structure Analysis of Landing Gear

The strength and weight are the major considerations for the UAV landing gear. In this study, simulations of the layered CFRP were performed using static structure analysis of Ansys Composite Pre-Post (ACP). The material properties are as follows: Young's modulus, E_1 = 160.8 GPa and E_2 = 11.9 GPa; Poisson's ratio, ν = 0.326; shear modulus, G = 6.8 GPa; density, ρ = 1530 kg/m^3; and yield stress, E_Y = 650 MPa. The formula used in ACP comes from the stress–strain relations for a lamina of arbitrary orientation, as shown in Figure 5. The transformation equations for stresses in an x–y coordinate system in terms of stresses in a 1–2 coordinates system are:

$$\left\{ \begin{array}{c} \sigma_{xx} \\ \sigma_{yy} \\ \tau_{xy} \end{array} \right\} = \left[\begin{array}{ccc} \cos^2\theta & \sin^2\theta & -2\sin\theta\cos\theta \\ \sin^2\theta & \cos^2\theta & 2\sin\theta\cos\theta \\ \sin\theta\cos\theta & -\sin\theta\cos\theta & \cos^2\theta - \sin^2\theta \end{array} \right] \left\{ \begin{array}{c} \sigma_{11} \\ \sigma_{22} \\ \tau_{12} \end{array} \right\} = [T]^{-1} \left\{ \begin{array}{c} \sigma_{11} \\ \sigma_{22} \\ \tau_{12} \end{array} \right\} \tag{1}$$

where θ is the rotational angle from the x-axis to the 1-axis. The strain transformation equations are:

$$\left\{ \begin{array}{c} \varepsilon_{xx} \\ \varepsilon_{yy} \\ \frac{\gamma_{xy}}{2} \end{array} \right\} = [T]^{-1} \left\{ \begin{array}{c} \varepsilon_{11} \\ \varepsilon_{22} \\ \frac{\gamma_{12}}{2} \end{array} \right\} \tag{2}$$

(**a**) principal material axes(1-2) and arbitrary x-y axes

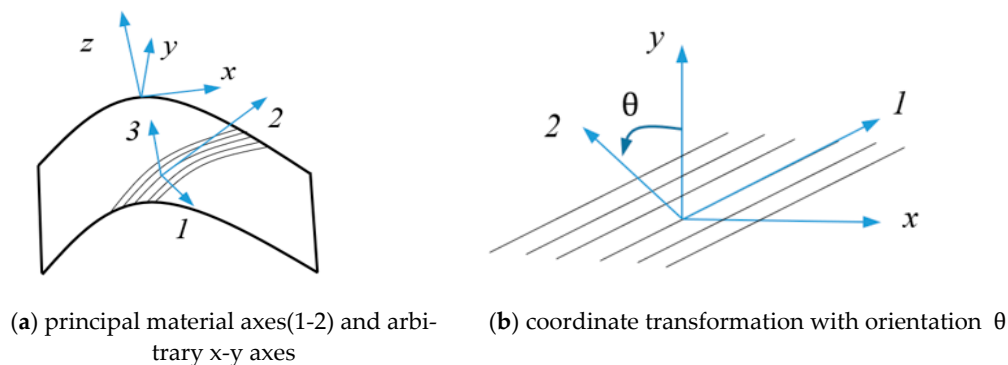(**b**) coordinate transformation with orientation θ

Figure 5. Positive rotation of principal material axes (1–2 axes) from arbitrary x–y axes.

The stress–strain relationships of composite materials in principal orientation are:

$$\left\{ \begin{array}{c} \sigma_{11} \\ \sigma_{22} \\ \tau_{12} \end{array} \right\} = \left[\begin{array}{ccc} Q_{11} & Q_{12} & Q_{16} \\ Q_{12} & Q_{22} & Q_{26} \\ Q_{16} & Q_{26} & Q_{66} \end{array} \right] \left\{ \begin{array}{c} \varepsilon_{11} \\ \varepsilon_{22} \\ \gamma_{12} \end{array} \right\} = [Q] \left\{ \begin{array}{c} \varepsilon_{11} \\ \varepsilon_{22} \\ \gamma_{12} \end{array} \right\} \tag{3}$$

where Q_{ij} is the reduced stiffness in terms of the material properties, E_i is the Young's modulus, and ν_{ij} is Poisson's ratio. The stress–strain relationships of composite materials in an x–y coordinate system are obtained by using Equations (1)–(3), as follows.

$$\left\{ \begin{array}{c} \sigma_{xx} \\ \sigma_{yy} \\ \tau_{xy} \end{array} \right\} = [T]^{-1}[Q][T]^{-T} \left\{ \begin{array}{c} \varepsilon_{xx} \\ \varepsilon_{yy} \\ \gamma_{xy} \end{array} \right\} = \left[\begin{array}{ccc} \overline{Q}_{11} & \overline{Q}_{12} & \overline{Q}_{16} \\ \overline{Q}_{12} & \overline{Q}_{22} & \overline{Q}_{26} \\ \overline{Q}_{16} & \overline{Q}_{26} & \overline{Q}_{66} \end{array} \right] \left\{ \begin{array}{c} \varepsilon_{xx} \\ \varepsilon_{yy} \\ \gamma_{xy} \end{array} \right\} \tag{4}$$

where $\overline{Q}_{ij}$ denotes the transformed reduced stiffness instead of the reduced stiffness Q_{ij}. In the ACP program, the natural coordinate system of the landing gear, the material properties, and the fiber principal direction of CFRP in each layer are defined and given.

To simulate landing, a load is applied vertically using the MTS and the ends of the landing gear are fixed by jigs supported by the MTS in the experiments. The boundary conditions are as follows: (1) fixed support at the two ends and (2) 150-N vertical load at the upper center surface of the landing gear.

In general, the yield stress of a composite material depends on its constituent fiber and matrix base. Additives and/or processing methods influence the yield stress. For example, the yield stresses of composites with steel, aluminum alloy, and magnesium alloy are 300–1100, 250–550, and 160–210 MPa, respectively. Table 2 shows the principal stresses for the CFRP landing gear designs with 8, 10, and 12 layers. If the yield stress of the CFRP is 650 MPa, stresses of 341.71 and 218.51 MPa exceed the constraint of a safety factor of 3. The 8 PLY and 10 PLY designs have the advantage of weight reduction; especially for 12 PLY, it is 39.3% heavier than 8 PLY. 10 PLY may be the choice if the safety factor is 2. In this study, the 12 PLY design is chosen. Table 3 presents the simulation results of different meshes to demonstrate the convergence. The last two results tend toward similar values as the mesh density increases. Table 4 shows the simulation results for designs with different fiber orientations in each layer. The single-axial fiber design for $[0]_{12}$ has great strength to support a pure vertical load. The design for $[0/90]_{6S}$ is the second best because it has more zero-degree layers than the $[0/90/45/-45/90/0]_S$ design.

Table 2. Simulations for number of layers landing gear.

CFRP Layers	Strain ε_{xx}	Stress σ_{xx} (MPa)	Factor of Safety	Displacement u_y (mm)	Weight (g)	Weight Reduction $\Delta W/avg$ (W)
$[0]_8$	21.111×10^{-4}	341.71	1.90	-3.9806	28	
$[0]_{10}$	10.335×10^{-4}	218.51	2.97	-2.0535	37	25.2%
$[0]_{12}$	9.371×10^{-4}	151.57	4.29	-1.1980	42	39.3%

Table 3. Grid independent analysis.

Node	Element	Strain ε_{xx}	Principal Stress σ_1 (MPa)	Displacement u_y (mm)	Meshed Landing Gear
43,215	40,629	9.841×10^{-4}	157.86	-1.250	
64,558	57,008	9.371×10^{-4}	151.57	-1.198	
240,699	21,720	9.385×10^{-4}	151.96	-1.198	

Table 4. Simulations for 12 layers landing gear of different fiber orientations.

CFRP Layers Design	Strain ε_{xx}	Principal Stress σ_1 (MPa)	Displacement u_y (mm)
$[0]_{12}$	9.371×10^{-4}	151.57	-1.198
$[0/90]_{6S}$	14.163×10^{-4}	229.41	-1.820
$[0/90/45/-45/90/0]_S$	17.910×10^{-4}	290.22	-2.273

Figure 6 shows the simulation result of maximum displacement u_y of the $[0/90]_{6S}$ design. If the aircraft lands improperly and is subjected to a side force of 150(cos30sin60, sin30, cos30con60) N, the additional loads along the x and z coordinates are borne by the fibers along the transverse directions. Table 5 shows that the axial normal strain ε_{xx} is minimal with fiber orientations of $\pm45°$ in the layers. The zero-degree orientation design still affords good strength against the y displacement and the overall principal strains.
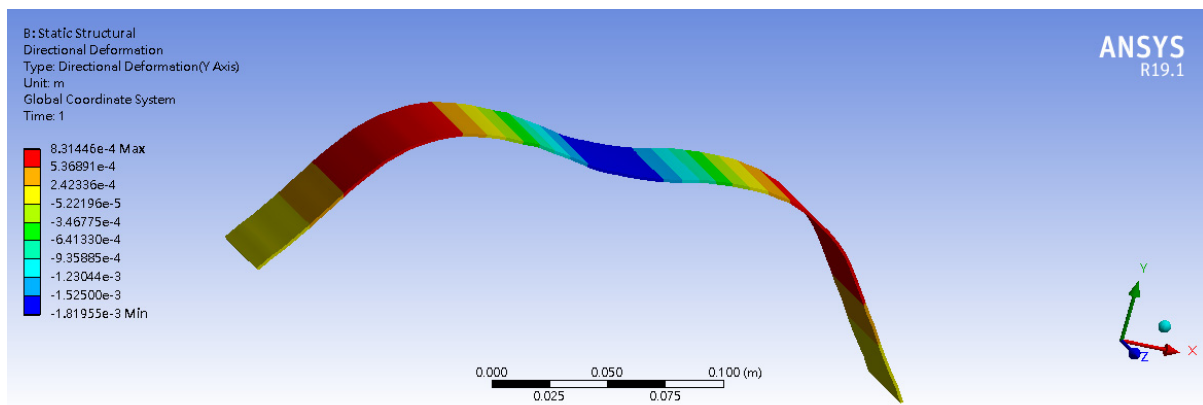
Figure 6. Vertical displacement u_y of the $[0/90]_{6S}$ design landing gear.

Table 5. Landing gear subject to side force loading.

Force 150N Component (x, y, z)	CFRP Layers Design	Strain ε_{xx}	Displacement u_y (Mm)	Max. Principal Strain	Min. Principal Strain
	$[0]_{12}$	1.970×10^{-4}	-1.868	2.8498×10^{-4}	-3.375×10^{-4}
$(-112.5, -75, -65)$	$[0/90]_{6S}$	1.791×10^{-4}	-3.829	22.376×10^{-4}	-22.966×10^{-4}
	$[0/90/45/-45/90/0]_S$	1.678×10^{-4}	-4.745	21.874×10^{-4}	-24.369×10^{-4}

4. Manufacture of Landing Gear

Once the curve of landing gear was defined, a steel mold was produced for compressing the CFRP, as shown in Figure 7a. The schematic description of laminate manufacture is shown in Figure 7b,c, showing the manufacturing processes. As shown in Figure 8a, the standard curing processes are 80 °C for 30 min in stage one and 120 °C for 90 min in stage two. The pressure is kept at 300 psi. At the low temperature in stage one, the CFRP is soft and mixes completely with the epoxy. At the high temperature in stage two, the form shape hardens. Figure 8b shows the final product. The manufacture quality of the landing gear is controlled stably by using the steel mold, and the manufacturing costs are reduced by using a mold that is affordable and allows hot-pressing many times.
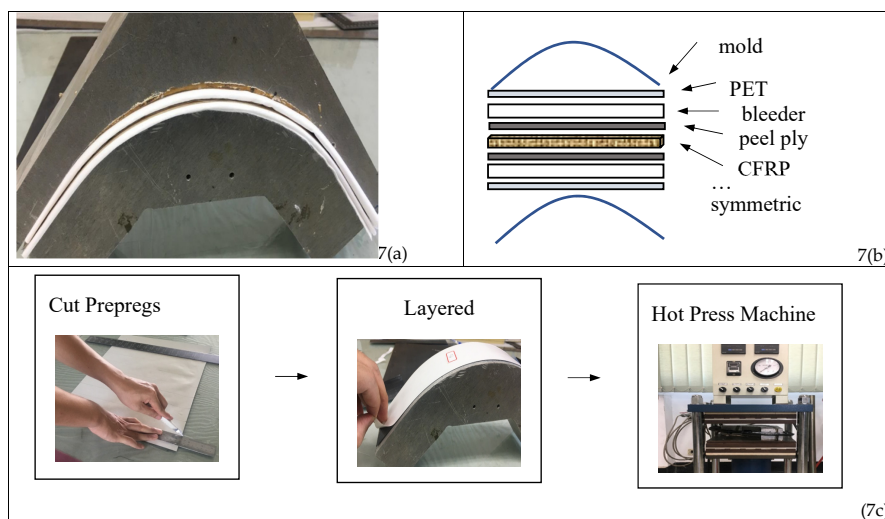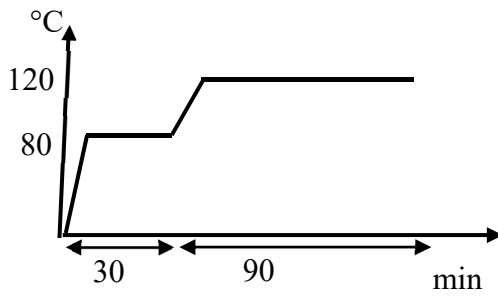

Figure 7. (**a**) Steel mold of UAV landing gear. (**b**) Schematic description of laminate manufacture. (**c**) Standard processes of carbon fiber-reinforced polymer (CFRP) landing gear manufacture.

(a) Curing process of CFRP.　　　　　　　　　　(b) The CFRP landing Gear (12 layers).

Figure 8. Product of CFRP landing gear.

5. Experiment Setup and Strain Measurement

5.1. Material Test Stand

The signal for strain gauge calibration and the setup of the NI-9237 data acquisition (DAQ) card are important factors in setting up the experiment. The measurement position on the landing gear must be cleaned before the KYOWA KFG-5-120-C1-11L5M2R strain gauge is glued. The displacement and load of the MTS should be returned to zero before conducting the experiments. The maximum load was set to 150 N, and the downward loading velocity was 1 mm/min. Figure 9 shows the load-time plot of the MTS.
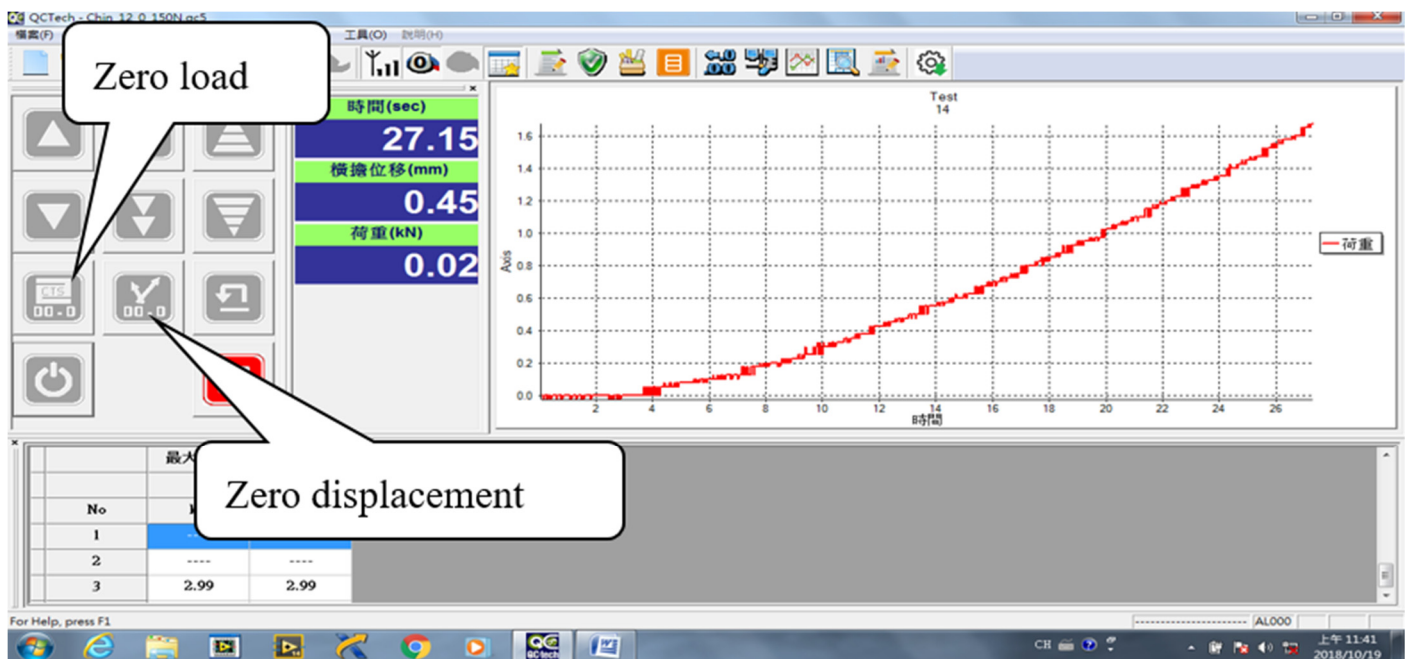

Figure 9. Loading process of material test stand (MTS). 時間means time, 橫擔位移means displacement, 荷重means load.

5.2. Strain Measured by NI9237

First, the strain gauge with the NI 9237 DAQ card and the NI 9945 adapter needed to be connected. The NI9945 adapter is in the quarter bridge I strain configuration. As shown in Figure 10a, pins 1 and 2 were connected, and the two lines of the strain gauge were connected to pins 0 and 1. As shown in Figure 10b, the adapter signal was sent to the NI9237 DAQ card. Before measuring the signal, the hardware must be detected using NIMax, and the device must be set up based on the manufacturer's specifications of strain gauge, as shown in Figure 11. The gage factor was 2.06 and the gage resistance was 120 Ω. Calibration must always be performed before conducting the experiments, as shown in Figure 12. The errors of channel 1 were calibrated to less than 1%. Figure 13 shows a block

diagram of the LabVIEW program. Figure 14 shows the front panel of strain measurements of the two channels. The data acquisition (DAQ) task was accomplished by strain gain, DAQ device (NI 9237, National Instruments, www.ni.com), and graphical programming language LabVIEW on PC. The virtual instrument of LabVIEW contains two windows: a front panel for the human–machine interface to control the instrument and indicate data, and a block diagram to process data by data flow paradigm. The sampling rate was set to be 25,000 Hz and the number of samples was specified as 2500 points. Every 0.1 s, the mean values of strain were calculated and presented on the front panel in real time.
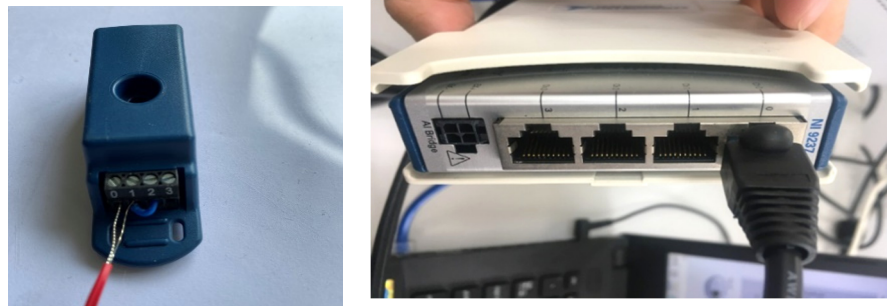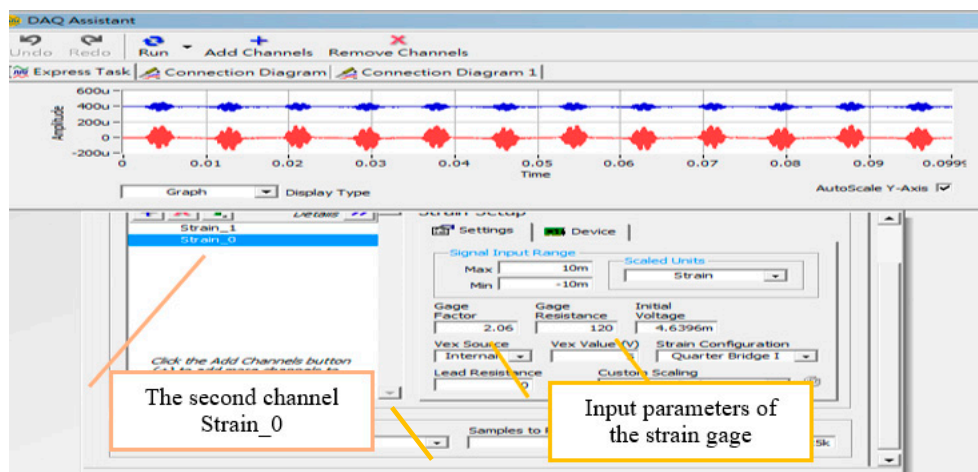

Figure 10. Instruments of strain measurement.
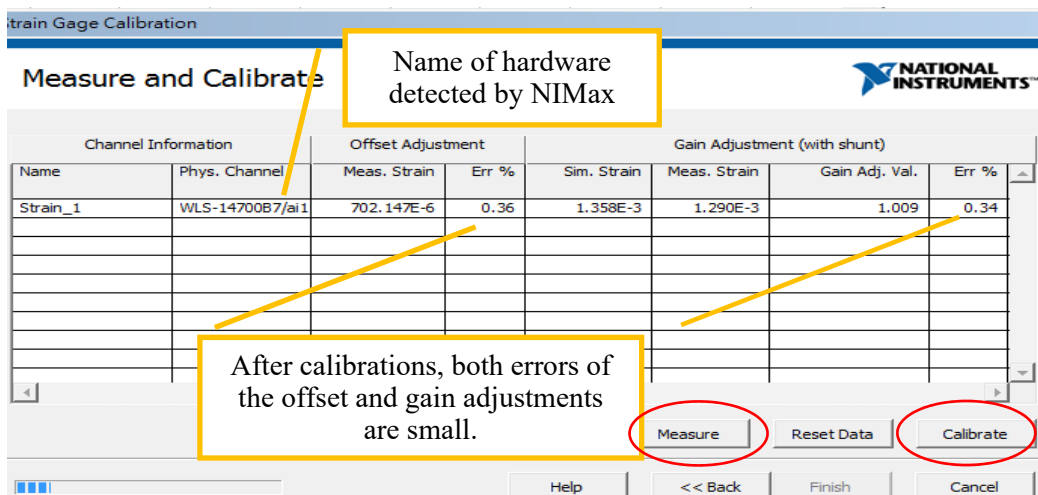

Figure 11. Device settings of strain gauge.

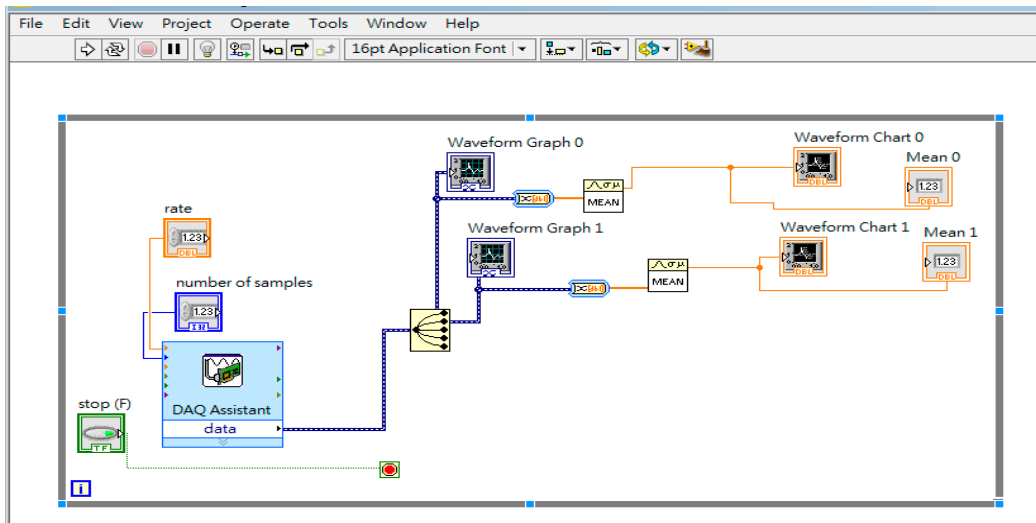**Figure 12.** System calibration before experiments (channel 1).

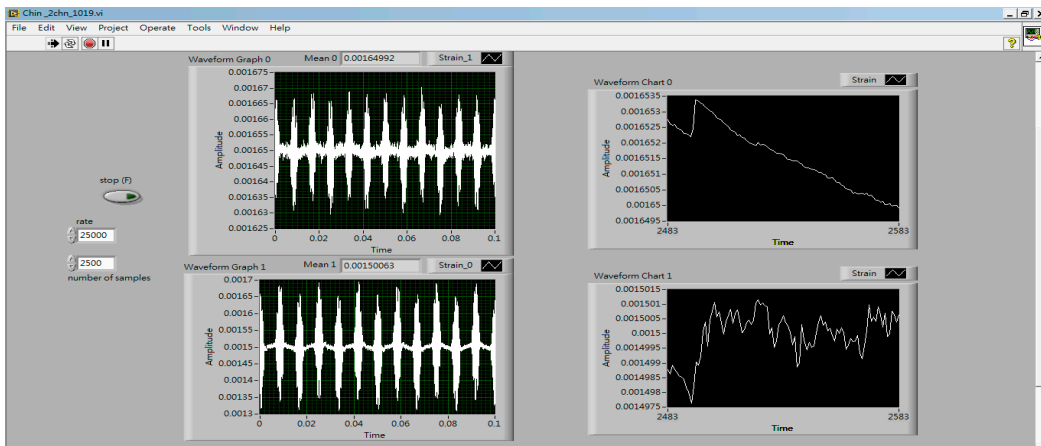**Figure 13.** The block diagram of LabVIEW (two channels).

Figure 14. The front panel of two channels' strain measurements.

5.3. Measurement Error

Accurate measurement results require reliable measurement equipment. The precision decreases with improper operation of the MTS machine, poor calibration of the DAQ card, or imperfect attachment of sensors. The errors between the measured data are defined as follows:

$$\varepsilon_i = \bar{\varepsilon} + RMSE, \tag{5}$$

where

$$\bar{\varepsilon} = \frac{\sum_{i=1}^{n} \varepsilon_i}{n} \tag{6}$$

$$RMSE = \sqrt{\frac{\sum_{i=1}^{n} \Delta\varepsilon_i^2}{n}}, \ \Delta\varepsilon_i = \varepsilon_i - \bar{\varepsilon} \tag{7}$$

n is the number of measurements, ε_i is the ith measured strain, $\bar{\varepsilon}$ is the average of the measured strains, and $\Delta\varepsilon_i$ is the difference between the averaged value and measured data.

6. Results and Discussions

This study conducted numerical analyses and experimental measurements of various CFRP landing gear designs. Table 6 presents the measurement errors calculated using Equations (5)–(7) for the $[0/90]_{6S}$ design. The first two columns of Table 7 show the strain

measurements and numerical simulation results for the $[0]_{12}$ 12-layered CFRP landing gear to check the accuracy of our problems. The 3D model refers to the simulation conducted by setting the thickness of the landing gear to the sum of the thicknesses of the 12 layers and meshing using 3D meshes. ACP refers to the simulation conducted using ACP modeling. This table also shows the results for the $[0/90]_{6S}$ and $[0/90/45/-45/90/0]_S$ fiber orientations. The results are reliable with errors less than 5%. The errors may arise from the force application position during the experiment, loosened fixed support of the jigs, and signal acquisition noise; errors can be reduced through multiple calibrations and good connections of strain gauges.

Table 6. Measurement error of strains for the $[0/90]_{6S}$ design.

	ε_{xx}	$\bar{\varepsilon}$ (RMSE)
First measurement	14.08×10^{-4}	
Second measurement	16.08×10^{-4}	13.86×10^{-4} (1.91%)
Third measurement	11.41×10^{-4}	

Table 7. Simulations and experiment results of strains.

CFRP Landing Gear	$[0]_{12}$ (3D Model)	$[0]_{12}$ (ACP)	$[0/90]_{2S}$	$[0/90/45/-45/90/0]_S$
Simulation ε_{xx}	8.7514×10^{-4}	9.371×10^{-4}	14.163×10^{-4}	17.910×10^{-4}
Experiment ε_{xx}	9.0×10^{-4}		13.86×10^{-4}	18.53×10^{-4}
Error	2.76%	4.12%	2.21%	3.35%

7. Conclusions

UAV landing gear should have low weight and high strength. This study designed 8 PLY, 10 PLY, and 12 PLY landing gears with different fiber orientations of CFRP for curved landing gear of a UAV with 5-kg weight and 10-kg maximum payload. Moreover, numerical simulations were conducted, a landing gear was manufactured, and experimental strain measurements were performed. The following conclusions can be drawn from this study.

1. Landing gear with a non-curved design has almost two times the stress concentration of landing gear with a curved design. A design without corners is the first choice for the landing gear of a UAV because it must withstand take-off and landing with continuous duty and short-time loading.

2. Considering the requirement of a safety factor of 3, implying that the design can withstand an accident with a heavy landing exceeding 3 g, the 8 PLY and 10 PLY CFRP designs are good in weight reduction except if the factor of safety is lower than 3. A design with more than 12 layers meets this requirement.

3. The simulation and experimental results show good agreement. The 12-layer zero-degree design $[0]_{12}$ has high strength when subjected to a pure vertical load. The next best design is $[0/90]_{6S}$. The $[0/90/45/-45/90/0]_S$ design shows good longitudinal strain when subjected to side forces. For products with a longitudinal design, such as the landing gear, fuselage, and wing of an aircraft, high strength is mainly afforded by fibers along the longitudinal direction.

Author Contributions: Conceptualization, methodology, numerical analysis, and writing—original draft preparation, Y.-C.L.; manufacture, experiment, and measurement setup, P.-C.C. and Y.-P.S.; writing—review and editing, M.-R.W. All authors have read and agreed to the published version of the manuscript.

Institutional Review Board Statement: Not applicable.

Acknowledgments: The authors would like to thank Ching-Rong Lee and Jih-Lung Lin for assisting with the mold manufacture.

Conflicts of Interest: The authors declare no conflict of interest.

References

1. Outay, F.; Mengash, H.A.; Adnan, M. Applications of unmanned aerial vehicle (UAV) inroad safety, traffic and highway infrastructure management: Recent advances and challenges. *Transp. Res. Part A Policy Pract.* **2020**, *141*, 116–129. [CrossRef] [PubMed]
2. Mammarella, M.; Comba, L.; Biglia, A.; Dabbene, F.; Gay, P. Cooperative agricultural operations of aerial and ground unmanned vehicles. *IEEE Int. Workshop Metrol. Agric. For.* **2020**, 224–229. [CrossRef]
3. Mohamed, N.; Al-Jaroodi, J.; Jawhar, I.; Idries, A.; Mohammed, F. Unmanned aerial vehicles applications in future smart cities. *Technol. Forecast. Soc. Chang.* **2020**, *153*, 119293. [CrossRef]
4. Sudhakar, S.; Vijayakumar, V.; Kumar, C.S.; Priya, V.; Ravi, L.; Subramaniyaswamy, V. Unmanned aerial vehicle (UAV) based forest fire detection and monitoring for reducing false alarms in forest-fires. *Comput. Commun.* **2020**, *149*, 1–16. [CrossRef]
5. Chung, D.D.L. Mechanical properties. In *Composite Materials: Science and Applications*, 2nd ed.; Springer: New York, NY, USA, 2010; pp. 49–61.
6. Anand, K.V.; Neeraj, K.P.; Rajesh, N.; Prateek. Challenge and advantage of materials in design and fabrication of composite UAV. In *IOP Conference Series: Materials Science and Engineering*; IOP Publishing: Bristol, UK, 2018; Volume 455, p. 012005.
7. ElFaham, M.M.; Mostafa, A.M.; Nasr, G.M. Unmanned aerial vehicle (UAV) manufacturing materials: Synthesis, spectroscopic characterization and dynamic mechanical analysis (DMA). *J. Mol. Struct.* **2020**, *1201*, 127211. [CrossRef]
8. Thuis, B.G.S.J. The Development of Composite Landing Gear Components for Aerospace Applications. In Proceedings of the 63rd Annual Conference of Society of Allied Weight Engineers, Newport Beach, CA, USA, 17–19 May 2004; National Aerospace Laboratory NLR: Amsterdam, The Netherlands, 2004; NLR-TP-2004-141.
9. Park, Y.; Nguyen, K.H.; Kweon, J.; Choi, J.; Han, J.S. Structural analysis of a composite target-drone. *Int. J. Aeronaut. Space Sci.* **2011**, *12*, 84–91. [CrossRef]
10. Kshitij, S. Composite skid landing gear design feasibility. *J. Am. Helicopter Soc.* **2009**, *54*, 4. [CrossRef]
11. Pitatzis, N.; Savaidis, G.; Panagiotou, P.; Yakinthos, K. Design and FE calculations of a lightweight civil unmanned aerial vehicle. In Proceedings of the 58th ILMENAU Scientific Colloquium, Technische Universität Ilmenau, Ilmenau, Germany, 8–12 September 2014.
12. Thompson, D.J.; Feys, J.; Filewich, M.D.; Abdel-Magid, S.; Dalli, D.; Goto, F. The design and construction of a blended wing body UAV. In Proceedings of the 49th AIAA Aerospace Sciences Meeting including the New Horizons Forum and Aerospace Exposition, Orlando, FL, USA, 4–7 January 2011.
13. Airoldi, A.; Bettini, P.; Boiocchi, M.; Sala, G. Composite elements for biomimetic aerospace structures with progressive shape variation capabilities. *Adv. Technol. Innov.* **2016**, *1*, 13–15.
14. Ciobanu, I.; Drăguș, L.; Țigleanu, L.; Frunză, C.; Bălăuță, D.; Olaru, S. Manufacturing of a landing gear using composite materials for an aerial target. *J. Phys. Conf. Ser.* **2019**, 1–10. [CrossRef]
15. Parmar, J.; Acharya, V.; Challa, D.J. Slection and analysis of the landing gear for unmanned aerial vehicle for SAE aero design series. *Int. J. Mech. Eng. Technol. IJMET* **2015**, *6*, 10–18.